NANO · MICRO small
www.small-journal.com

Probing Effective Out-of-Plane Piezoelectricity in van der Waals Layered Materials Induced by Flexoelectricity

Xiang Wang, Anyang Cui, Fangfang Chen, Liping Xu, Zhigao Hu, Kai Jiang, Liyan Shang, and Junhao Chu*

Many van der Waals layered 2D materials, such as *h*-BN, transition metal dichalcogenides (TMDs), and group-III monochalcogenides, have been predicted to possess piezoelectric and mechanically flexible natures, which greatly motivates potential applications in piezotronic devices and nanogenerators. However, only intrinsic in-plane piezoelectricity exists in these 2D materials and the piezoelectric effect is confined in odd-layers of TMDs. The present work is intent on combining the free-standing design and piezoresponse force microscopy techniques to obtain and directly quantify the effective out-of-plane electromechanical coupling induced by strain gradient on atomically thin MoS_2 and InSe flakes. Conspicuous piezoresponse and the measured piezoelectric coefficient with respect to the number of layers or thickness are systematically illustrated for both MoS_2 and InSe flakes. Note that the promising effective piezoelectric coefficient (d_{33}^{eff}) of about 21.9 pm V^{-1} is observed on few-layered InSe. The out-of-plane piezoresponse arises from the net dipole moment along the normal direction of the curvature membrane induced by strain gradient. This work not only provides a feasible and flexible method to acquire and quantify the out-of-plane electromechanical coupling on van der Waals layered materials, but also paves the way to understand and tune the flexoelectric effect of 2D systems.

1. Introduction

The rapid developments of microelectromechanical systems (MEMS)[1,2] and nanoscale electronics demand high-performance piezotronic devices to be miniaturized. 2D piezoelectric materials are ideal candidates due to their superior electronic properties[3–8] and the mechanically flexible nature.[9–12] Since Wu et al. first observed piezoelectricity of monolayer MoS_2 by fabricating a flexible generator,[13] piezoelectric investigations of novel atomically thin materials have attracted extensive attentions. Indeed, many 2D layered materials, such as *h*-BN, transition metal dichalcogenides (TMDs), and group-III monochalcogenides (MX, M = Ga and In, X = S, Se, and Te), have been theoretically predicted to be piezoelectric.[14–20] These 2D piezoelectric materials with the D_{3h} ($\bar{6}$m2) point group are fundamentally predicted by the group theory to only possess nonzero in-plane piezoelectric coefficients.[14,20] When a strain gradient is added along the out-of-plane direction, it can induce the electric polarization along the same direction and contribute to additional electromechanical coupling, referred to as flexoelectricity.[21–28] Free-standing structure is a classical strategy on studying mechanical properties of 2D materials.[10,12,29–32] Electronic bandgap and optical properties of 2D materials also could be tunable via strain engineering.[33–35] Here, we adopt the suspension structure to yield large deformation and induce flexoelectric effect on free-standing 2D materials.

Scanning probe microscopy (SPM) techniques, i.e., piezoresponse force microscopy (PFM) and conductive atomic force microscope (C-AFM) have been considered as the preferred tools to dissect the extremely weak electromechanical phenomenon of low-dimensional materials. Piezoelectric effect of 2D materials can be achieved by collecting the mechanical strain induced voltage or current alteration on piezoelectric devices.[36–41] A method combining a laterally applied electric field and nanoindentation technique was employed to observe piezoelectricity in free-standing MoS_2.[42] Esfahani et al. have measured the effective electromechanical coefficient of monolayer WSe_2 on a substrate as 5.2 pm V^{-1} based Possion's effect through a laterally excited SPM mode.[43] Picoampere scale electric current from the suspended MoS_2 has been observed *via* C-AFM.[44,45] PFM mode is generally regarded as a powerful and direct way to characterize the piezoelectric and ferroelectric properties by applying an out-of-plane electric field to excite the sample through a conductive probe.[46–49] Although there are sufficient attention and significant progress, it is

Dr. X. Wang, Dr. A. Y. Cui, Dr. F. F. Chen, Dr. L. P. Xu, Prof. Z. G. Hu, Dr. K. Jiang, Dr. L. Y. Shang, Prof. J. H. Chu
Technical Center for Multifunctional Magneto-Optical Spectroscopy (Shanghai)
Department of Electronic Engineering
East China Normal University
Shanghai 200241, China
E-mail: zghu@ee.ecnu.edu.cn
Prof. Z. G. Hu, Prof. J. H. Chu
Collaborative Innovation Center of Extreme Optics
Shanxi University
Taiyuan 030006, Shanxi, China
Prof. Z. G. Hu, Prof. J. H. Chu
Shanghai Institute of Intelligent Electronics and Systems
Fudan University
Shanghai 200433, China
The ORCID identification number(s) for the author(s) of this article can be found under https://doi.org/10.1002/smll.201903106.

DOI: 10.1002/smll.201903106

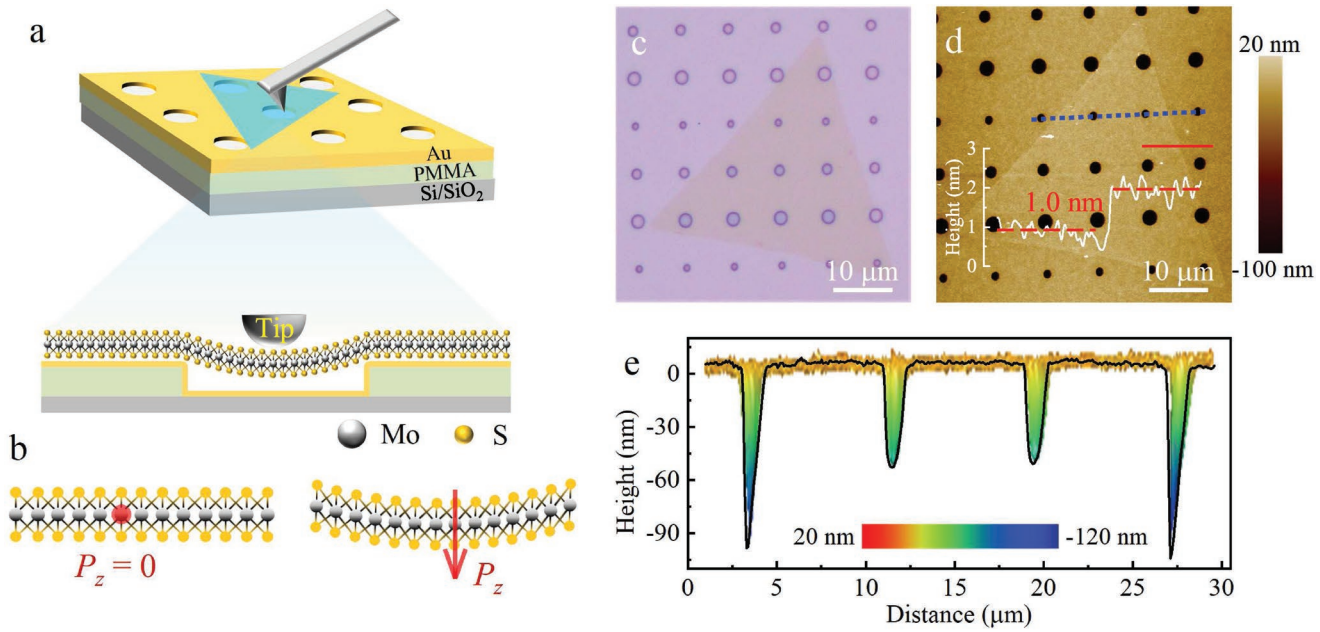

Figure 1. a) The schematic representation of the experimental configuration involving AFM probe (top) and the magnifying side view of the possible crystal structures of suspended MoS_2 flake (bottom). b) The side view of normal polarization in flat and bent MoS_2 flake. c) The optical microscopy image and d) AFM topography of monolayer MoS_2 triangular monocrystal upon the perforated substrate. The inset is height profile along the red solid line in (d). e) The section view and height profile along the blue dotted line in (d).

still challenging to directly observe the piezoelectric response on atomically thin materials. Recently, PFM has been used to detect out-of-plane electromechanical coupling induced by flexoelectricity on 2D TMDs. The effective out-of-plane piezoelectric coefficient (d_{33}^{eff}) of monolayer MoS_2 on a flat substrate has been reported as 1.12 pm V^{-1}.[50] Then, the d_{33}^{eff} of thin-layered corrugation $MoTe_2$ was obtained as 3.98 pm V^{-1}.[51] However, strain-gradient effect induced by substrate for the supported 2D system is technically restricted and ambiguous. And some negative effects, such as clamping effect, parasitic charges, and doping effect, would be inevitably derived from the substrate.[42,51–53] The unexpectable experimental error of PFM resulting from the complicated substrate effects should be avoided in 2D piezoelectric systems. Therefore, an improved technique for probing piezoresponse in atomically thin materials is particularly expected by distinguishing the contributions from intrinsic piezoelectricity or flexoelectricity, as well as eliminating strong negative effects.

In the present work, we have proposed a practical approach to directly obtain and detect the out-of-plane electromechanical coupling and the effective piezoelectric constant in free-standing monolayer to few-layered MoS_2 and thin-layered γ-InSe flakes. The utilization of suspended structure not only benefits to form large deformation but also could avoid the substrate effects so as to accurately determine the effective piezoelectric constant by PFM technique. Based on this kit of experimental configuration, we can observe an excellent piezoelectricity response of monolayer MoS_2 with the d_{33}^{eff} as about 7.5 pm V^{-1}. Moreover, we have first discovered promising d_{33}^{eff} coefficient of about 21.9 pm V^{-1} from thin-layered γ-InSe flakes. Furthermore, the roles of curvature and thickness on flexoelectric effect were discussed qualitatively. Our work would motivate the nanopiezotronics development of low-dimensional materials and their potential electronic applications.

2. Results and Discussion

2.1. Electromechanical Visualization of Free-Standing Monolayer MoS_2

The numbers of layers of few-layer MoS_2 flakes were concluded to be 1 to 10 layers from the peak positions of E_{2g}^1 and A_{1g} modes of Raman spectra and the height profiles of AFM morphologic maps,[54] as shown in Figure S1 in the Supporting Information. The thicknesses of thin-layered InSe flakes were also evaluated to be 4.8–95.0 nm by Raman spectra and AFM morphologic maps,[55] as shown in Figures S2 and S4 in the Supporting Information. Then, the morphology and the electromechanical properties of samples were studied by the PFM mode, whose experimental schematic diagram was shown in **Figure 1**a. The perforated substrate with matrix of holes was a three-layered structure containing silicon wafer at the bottom, 200–300 nm thick polymethylmethacrylate (PMMA) in the middle and Au layer with thickness of 50 nm at the top, as shown in Figure 1a. The top gold layer acted as the bottom electrode and could reduce the surface roughness of the substrate.

The ultrathin film is bent over the hole naturally after transferred on a perforated substrate. During the herein presented PFM measurements, the force loaded on the sample remained less than 10 nN. A small force of tip–sample interaction is not enough to change the curvature of naturally suspended membrane, and could avoid the additional mechanical contribution from the tip. The suspended structure could result in a natural

curvature in 2D crystal, so that a net dipole moment could be obtained along normal direction of the membrane.[22,26,51] In terms of monolayer MoS_2, polarization in normal direction can be induced at the bent region, as shown in the schematic of Figure 1b. The optical image and AFM topography of the triangular monolayer MoS_2 flake covering on the perforated substrate are shown in Figure 1c,d, respectively. The thickness of monolayer MoS_2 was determined to be 1.0 nm, as shown in the inset of Figure 1d. Figure 1e (the sectional view and height profile along the dotted blue line in Figure 1d) shows that the depths of covered and uncovered holes are about 50 and 100 nm, respectively. It indicated that the state of free-standing samples over the holes was consistent with the structure showed in the bottom of Figure 1a. The fundamental optical and AFM microscopic characterizations manifested that the suspended membranes were continuous and undamaged.

To determine the effective out-of-plane piezoelectric coefficient (d_{33}^{eff}), an alternating current (AC) modulation voltage was added to the conductive tip to induce the vertical piezoresponse displacement of sample, where the lock-in amplification technique was used to measure the weak PFM piezoresponse. The driven piezoresponse displacement, A_P (pm), is the product of the detected vertical deflection voltage V_P (mV) versus deflection sensitivity of the cantilever δ (nm V^{-1}),[56,57] given by $A_P(\text{pm}) = V_P \times \delta$. Further, the observed value of d_{33}^{eff} can be determined by [58]

$$d_{33}^{\text{eff}} = \frac{A_P(\text{pm})}{V_{AC}(\text{V})} \quad (1)$$

where V_{AC} (V) is the amplitude of the applied AC driving voltage.

Figure 2a displays the topographic map of the monolayer MoS_2 membrane suspended on a single hole and inset is the line scan along diameter of hole, whose diameter is 2.44 μm. The integrity and continuity of the MoS_2 film could be confirmed from the topographic map. The free-standing areas have inflected into the same shape of the bottom of a round bowl with a depth of 72.2 nm. Note that piezoresponse measurements were carried out on this region. Figure 2b–d presents the PFM amplitude images of single layer MoS_2 under various driving voltages of 0, 0.5, and 2 V. The insets represent the statistical distribution of the piezoresponse amplitude variations of bent and flat MoS_2. The piezoresponse histogram mapping in Figure 2b shows that a noise signal with the sub-picometer magnitude can be detected with no drive voltage (V_{AC} = 0 V). There was no difference in piezoresponse mapping between the supported and free-standing areas under zero drive bias. It is attributed to the fact that electromechanical displacement is not induced in the absence of an external electric field, even if a strain-gradient induced dipole moment existed in bent MoS_2 region. In contrast, the obvious amplitude distinction can be seen between the bent and flat MoS_2 under non-zero driving voltages. Piezoresponse amplitude increased steadily at the bent MoS_2 with increasing the drive bias, while the amplitude barely changed at flat regions. The piezoresponse statistical histograms present an effective piezoresponse at bent areas of about 3 ± 1.5 pm under 0.5 V drive voltage and of about 18 ± 3.5 pm at 2 V drive bias. The corresponding signal is approximately at the range from sub-picometer magnitude to several picometers at flat regions under 0.5 and 2 V bias, respectively. On the contrary, piezoresponse histogram profile demonstrates that the out-of-plane polarization can be observed with a stronger response at curvature MoS_2 regions than that at flat MoS_2. Namely, PFM could spontaneously collect the piezoresponse direction into the phase signal, where the signal of ±90° represents the antiparallel polarization. The corresponding piezoresponose phase images of monolayer MoS_2 are shown in Figure S3 in the Supporting Information. Similarly, no phase signal was probed at both bent and flat regions for the zero voltage of modulation. When the modulation voltage is set as over 0 V, the uniform phase response at the suspended area represents the existence of out-of-plane electromechanical coupling with a unified polarization direction for the bent monolayer MoS_2 flake.

In order to quantify the effective magnitude of observed piezoelectricity, the piezoresponse amplitudes in the areas of bent and flat monolayer MoS_2 have been averaged over the amplitude mapping, respectively. Then the piezoresponse amplitudes were plotted as a function of applied AC voltage, as shown in Figure 2e. The value of d_{33}^{eff} is independent of the applied AC amplitude. According to Equation (1), the d_{33}^{eff} coefficient of bent and flat MoS_2 can be obtained from the slope of the linear fitting curve in Figure 2e. We found that the bent monolayer MoS_2 presented the noticeable d_{33}^{eff} value of 7.5 pm V^{-1}, which is larger than those of wurtzite GaN (d_{33}^{eff} = 3.1 pm V^{-1})[59] and wurtzite AlN (d_{33}^{eff} = 5.1 pm V^{-1}).[59] One possible origin of the remarkable piezoelectric coefficient was the flexoelectricity induced by strain gradient. Compared with the unconspicuous effect of flexoelectric on 3D bulk materials, it becomes stronger on low-dimensional ones.[26,27] Moreover, the out-of-plane polarization of bent monolayer MoS_2 is dependent on the out-of-plane bending,[60] contributing to strong vertical electromechanical coupling. Notably, there was also a small d_{33}^{eff} coefficient with the value of 0.6 pm V^{-1} measured at flat MoS_2 regions. The weak electromechanical response of flat MoS_2 can be attributed to the tip and surface electrostatic interaction since there are neither intrinsic out-of-plane piezoelectricity nor flexoelectricity induced by strain gradient. The vertical electromechanical coupling of MoS_2 flakes with different layers was further investigated in Figure 2f. The d_{33}^{eff} coefficients can be collected within the magnitude range from 7.5 to 2.0 pm V^{-1} for 1 to 10 layers MoS_2 films. The specific numerical values of diameters of holes, bending depths of suspended membranes, and d_{33}^{eff} coefficients of 1 to 10 layers MoS_2 flakes are given in **Table 1**. It is generally accepted that the flexoelectricity of atomically thin MoS_2 is different from the intrinsic in-plane piezoelectricity, and is not restricted by odd number of layers. The effective piezoelectric coefficient obviously dropped off with the number of layers increasing. It could be inferred to the enhancement of flexoelectric effect with the decreasing of flake thickness.[51,61] The thickness dependence of flexoelectric effect on few-layer MoS_2 will be disscussed further in the later chapters.

2.2. Curvature and Thickness Tuning Piezoelectricity of Thin-Layered InSe

The effective out-of-plane piezoelectric coefficient could not only be obtained in TMDs class, such as atomically thin MoS_2.

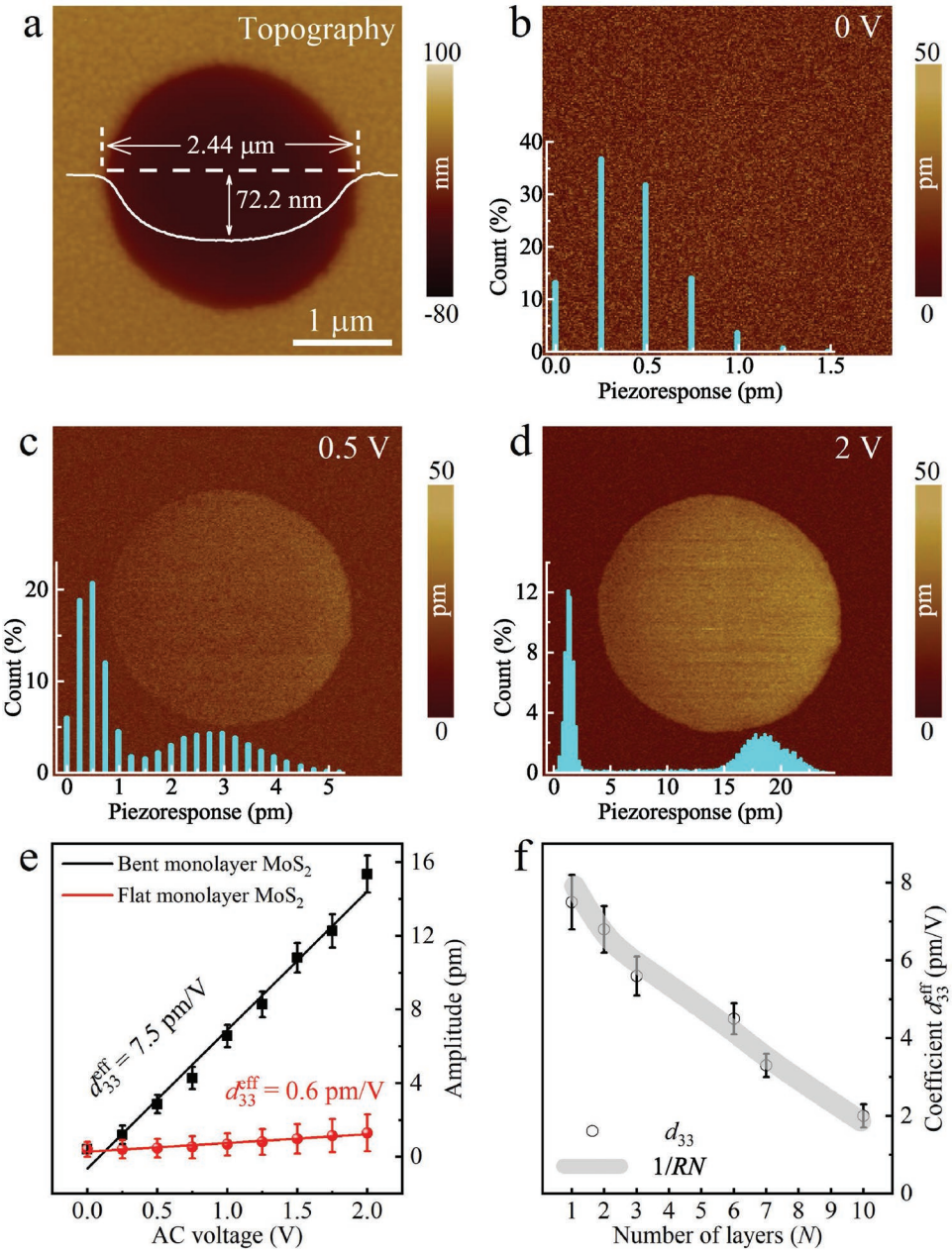

Figure 2. a) The AFM topography of monolayer MoS_2 suspended on the single hole. The inset is the line scan along diameter of hole. Out-of-plane piezoresponse amplitude images of monolayer MoS_2 under the drive voltage of b) 0 V, c) 0.5 V, and d) 2 V, respectively. The insets represent the statistical distribution of the piezoresponse amplitude variations of bent and flat MoS_2. e) Average piezoresponse amplitude of bent and flat monolayer MoS_2 as a function of the applied AC voltage. The solid lines are the fitting lines obtained by the least-square method. f) d_{33}^{eff}-coefficients of bent MoS_2 flakes with different number of layers. The gray solid line represents the reciprocal of the product of curvature radius (R) versus number of layers (N).

It has also been verified in this study that the out-of-plane piezoelectricity of γ-InSe flakes with different thickness was carefully achieved. The γ-InSe layer unit consists of three sublayers, whose each layer stacks four closely packed monoatomic sheets in the sequence of Se–In–In–Se. The three sublayers are combined by van der Waals forces, and each four atom-thick monolayer held together mainly by covalent bonding with some ionic characteristics.[62] Group theory predicts that both monolayers of γ-InSe and 2H TMDC belong to the D_{3h} ($\bar{6}$m2) point group.[14,20] In the case of D_{3h}, only intrinsic in-plane piezoelectricity appears. That is the reason why the out-of-plane piezoelectric property of layered α-In_2Se_3 has been reported previously,[49,63] while the vertical piezoelectricity of γ-InSe has not been discovered up to now.

Here, we first observed the effective out-of-plane piezoelectricity in curvature γ-InSe flakes with the corresponding thickness from 4.8 nm few-layer to the thicker dimension of 95 nm. Typically, the piezoresponse amplitude images were collected on InSe sheets with the thickness of 7.5, 17.1, and 35.0 nm under different drive voltages as presented in **Figure 3**a–c, respectively.

Table 1. The curvature radii and d_{33}^{eff} coefficients of few-layer MoS_2 flakes and thin-layered InSe flakes.

Material	Number of layers N	Diameter of hole d_0 [μm]	Bending depth h [nm]	Curvature radius R [μm]	$1/(RN)$ (10^{-5} nm^{-1})	d_{33}^{eff} [pm V^{-1}]
MoS_2	1	2.44	72.2	10.3	9.7	7.5
MoS_2	2	1.70	55.1	6.6	7.6	6.8
MoS_2	3	1.24	39.0	5.0	6.8	5.6
MoS_2	6	1.20	45.6	4.0	4.2	4.5
MoS_2	7	1.12	34.6	4.5	3.2	3.3
MoS_2	10	1.60	24.2	13.2	0.7	2.0
Material	Thickness t [nm]	Diameter of hole d_0 [μm][a)]	Bending depth h [nm]	Curvature radius R [μm]	$1/(Rt)$ (10^{-5} nm^{-2})	d_{33}^{eff} [pm V^{-1}]
InSe	4.8	1.21	13.5	13.6	1.5	15.1
InSe	7.5	1.32	38.6	5.6	2.4	21.9
InSe	9.7	1.33	35.2	6.3	1.6	17.5
InSe	17.1	1.14	31.5	5.2	1.1	14.4
InSe	19.4	1.10	24.0	6.3	0.8	12.2
InSe	22.1	1.26	28.5	7.0	0.6	9.4
InSe	35.0	0.76	6.7	10.8	0.3	4.5
InSe	95.0	∞	0	∞	0	0.7

[a)]The symbol ∞ means that the numerical value approaches infinity.

Under zero-modulation, uniform signals of amplitude image and similar weak signals of piezoresponse histograms illustrate that the inevitable background noise exists, partially resulting from the measurement system. When an effective modulation voltage is given, the conspicuous piezoelectric amplitude response is observed at the bent areas of 7.5 and 17.1 nm thick InSe flakes. The piezoresponse statistical profile shows that the piezoresponse of curved InSe flakes is much stronger than that of flat regions, corresponding to the separated peaks located at low and high piezoresponse range, respectively. Note that the piezoelectric amplitude signals of flat regions of both 7.5 and 17.1 nm thick InSe flakes barely change with the increasing drive bias. It means that the electrostatic effect, which could be significantly weakened by using the stiff AFM cantilever with a spring constant of 3 N m^{-1},[64] could be ignored on thin InSe flakes. When InSe flake thickness increases to 35.0 nm, the statistical count cannot distinguish the signals of bent and flat regions any more due to the interference of noise signal. However, effective piezoelectric signal is still collected at bent regions, which could be certified by the evident distinctions at piezoresponse amplitude maps under high drive bias and the displacement of the peak of piezoresponse histograms. The results reveal again the chance of out-of-plane piezoelectricity induced by flexoelectricity in the curvature γ-InSe flakes, even if in-plane intrinsic piezoelectricity is purely allowed.

Furthermore, drive voltage dependent piezoelectric amplitude was plotted and used to determine the piezoelectric coefficient d_{33}^{eff} of InSe flakes in **Figure 4**a, where the curves were fitted well by a linear function. The corresponding experiment findings on 4.8 nm thick InSe are shown in Figure S4 in the Supporting Information. The d_{33}^{eff} coefficients can be obtained by examining the slopes of the linear fitting curves, and the associating coefficients can be seen in Figure 4b. The d_{33}^{eff} coefficients of InSe flakes gradually decrease from 21.9 to 0.7 pm V^{-1} with the sample thickness increasing from 7.5 to 95.0 nm, where this tendency is consistent with the thickness dependence of flexoelectric effect. However, the d_{33}^{eff} coefficient of 4.8 nm thick InSe is about 15.1 pm V^{-1}, which is smaller than the 21.9 pm V^{-1} of 7.5 nm thick InSe. This phenomenon corresponds to an anomalous correlation between thickness and piezoresponse strength. Thus it also points out that the flexoelectricity induced by bending should be relevant to other parameters. Actually, in addition to thickness effect, curvature radius or bending degree is another decisive factor affecting the strength of flexoelectric coupling.[27,60,65] All specific numerical values of diameters of holes, bending depths of suspended membranes, and d_{33}^{eff} coefficients of InSe flakes with variation thickness are given in Table 1. The diameters of suspended 4.8 and 7.5 nm thick InSe flakes are about 1.21 and 1.32 μm, respectively. And the bending depths are about 13.5 and 38.6 nm of 4.8 and 7.5 nm thick InSe flakes, respectively. Hence, the curvature radii of 4.8 and 7.5 nm thick InSe flakes are calculated to be ≈13.6 and 5.6 μm, respectively. More detailed discussion about the relation between curvature and flexoelectricity will be expanded later. Besides, the measured small piezoelectric coefficient of 0.7 pm V^{-1} without perceptible deformation is collected on the suspended 95.0 nm thick InSe flake. It may consider the extremely weak PFM signal to be partially derived from electrostatic interaction between the PFM tip and sample. Even for 35.0 nm thick InSe flake, the measured piezoelectric coefficient of 4.5 pm V^{-1} is much larger than 0.7 pm V^{-1}. Therefore, it indicates that the electrostatic effect is slight for thin InSe flakes.

Note that the effective piezoelectricity of InSe flakes presented a wider variation range from 21.9 to 4.5 pm V^{-1}, while

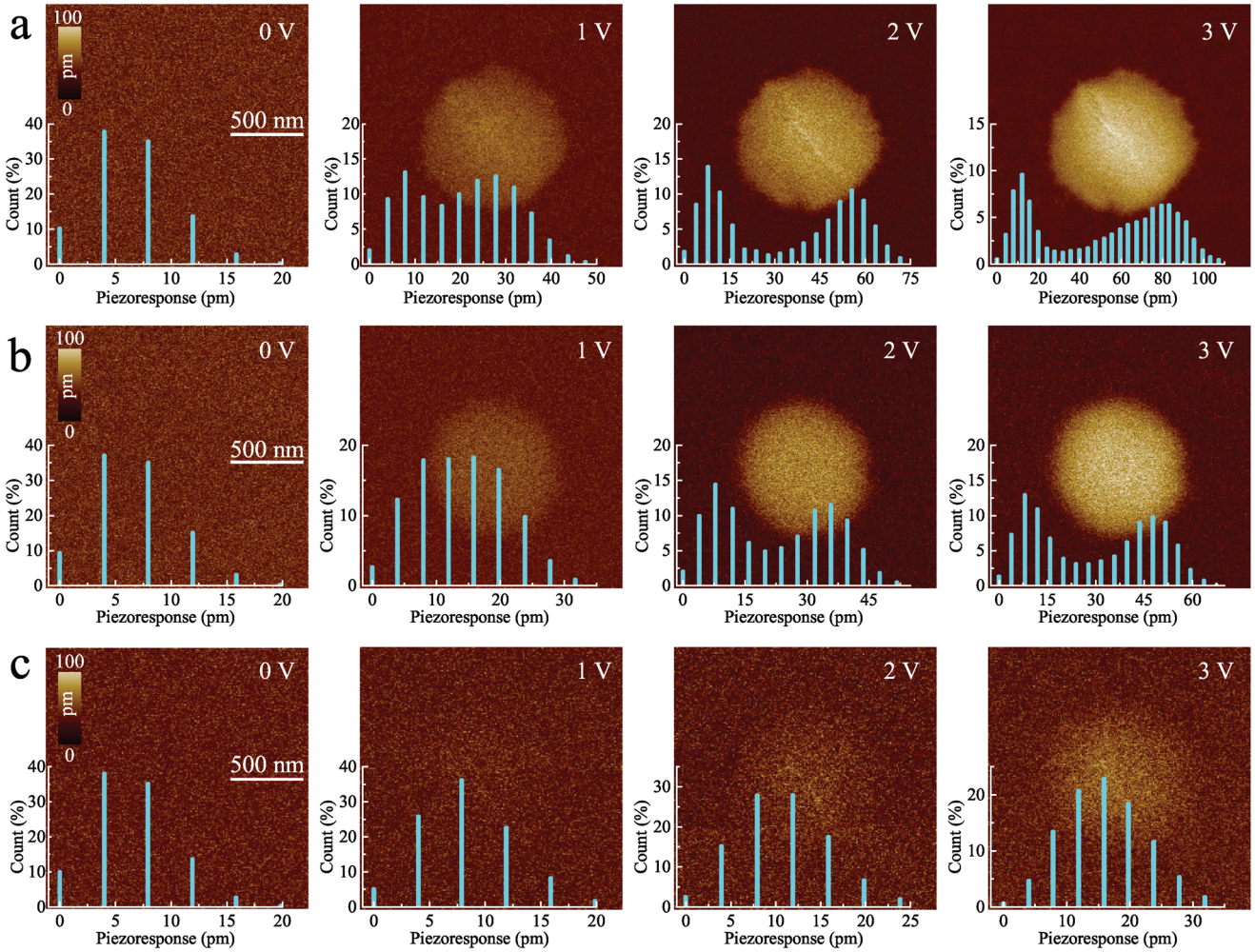

Figure 3. Out-of-plane piezoresponse amplitude images of a) 7.5 nm, b) 17.1 nm, and c) 35.0 nm thick InSe bent membranes under different drive voltages of 0, 1, 2, and 3 V, respectively. The insets represent the statistical distribution of the piezoresponse amplitude variations of bent and flat InSe flakes.

the variation range of MoS_2 was covered from 7.5 to 2.0 pm V^{-1}. This might be related to the intrinsic properties of selected materials. First, compared with 2H-MoS_2, γ-InSe possesses more complicated stacking behavior along the *c*-axis and various covalent bonds in different directions. Namely, the crystal atom of InSe is surrounded by more asymmetric energy distribution fields. Hence, dipoles induced by bending are easier to generate in InSe than in MoS_2. Furthermore, the dielectric constant of InSe[66] is higher than that of MoS_2.[67] Generally, the high dielectric constant materials probably correspond to strong electromechanical response.[68] Additionally, the diverse elastic coefficients of MoS_2 and InSe could be regarded as an another aspect on the difference of the effective piezoelectric property.[10,69] Materials with the greater out-of-plane piezoresponse generally possess a smaller elastic coefficient (c_{11}). For bulk dielectric materials, the relationship between the d_{33}^{eff} generated by flexoelectric effect and c_{11} can be expressed as $d_{33}^{\text{eff}} = \mu_{11}\frac{\nabla_3 T_3}{c_{11}T_3'}$, where μ_{11} is the flexoelectric coefficient of dielectric material, $\nabla_3 T_3$ is the stress gradient in the *z*-axis and T_3' is the stress along the *z*-axis.[24,26]

In **Table 2**, we highlight the comparison of the measured piezoelectric coefficients on various van der Waals layered materials (MoS_2 and InSe) between the previous reports and this work. Obviously, the out-of-plane piezoelectric coupling of 2D materials induced by flexoelectricity could be much stronger than the intrinsic in-plane piezoelectricity.[14,20] Effective d_{33} induced by flexoelectricity on monolayer MoS_2 supported by Al_2O_3 substrate was 1.35 ± 0.24 pm V^{-1} reported by Brennan et al.[50] On corrugated thin-layered $MoTe_2$, effective out-of-plane piezoelectricity was measured as 3.98 pm V^{-1} by Kang et al.[51] In our work, the free-standing structure benefits the observation of the piezoresponse by amplifying the strain gradient as well as avoiding the clamping effect. On the basis of the comparison in Table 2, note that the larger value of the measured d_{33}^{eff} coefficient has been obtained in this work, associating with the enhanced flexoelectric coupling.

The strength of flexoelectric coupling in bent 2D materials not only enhances with the decreasing sample thickness, but also depends on the bending degree. For a curved membrane, the curvature-induced polarization can be estimated as $P_s = f/R$,

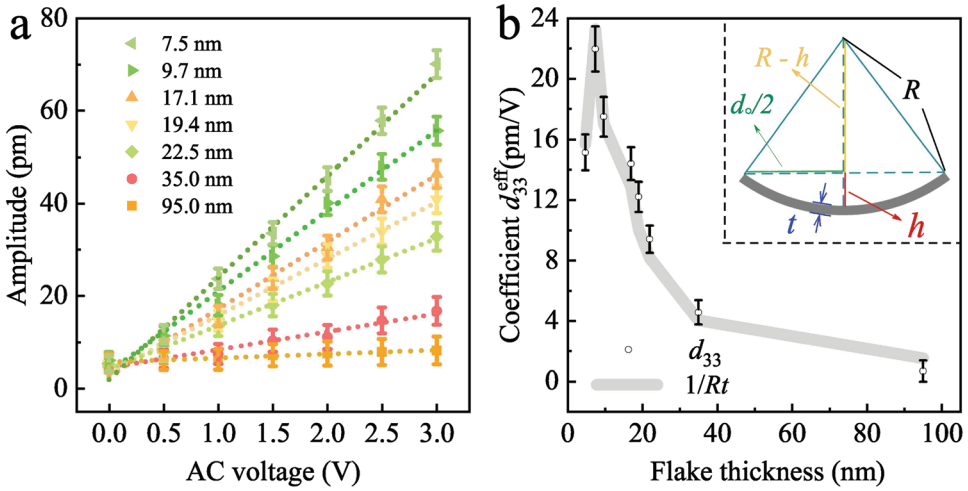

Figure 4. a) Average piezoresponse amplitude of the bent areas of different thickness InSe flakes as a function of the applied AC voltage. b) d_{33}^{eff} of bent InSe flakes with different thicknesses from 4.8 to 95.0 nm. The gray solid line represents the reciprocal of the product of curvature radius (R) versus sample thickness (t). The inset presents schematic of bent membrane and definition of each parameter for curvature radius calculation.

where P_s is the electric polarization per unit area (in C m^{-1}), R is the principal radius of curvature, and f is the flexoelectric constant.[27,60,65] Moreover, flexoelectric polarization (P_z) along z-axis has been previously reported to be proportional to the reciprocal of the sample thickness in bulk materials, such as square truncated pyramid structure.[24,65] The similar thickness dependence of flexoelectricity has also been reported in thin-layered $MoTe_2$.[51] Note that flexoelectricity of a curved membrane relies on both the bending degree and the thickness of sample. Therefore, the P_z of a curved membrane can be derived as $P_z \propto \frac{1}{Rt}$, where t is the thickness of membrane. Note that the vertical deflection voltage (V_P) for PFM probing system is determined by the perpendicular electric polarization of sample. Namely, the effective piezoelectric coefficient d_{33}^{eff} is proportional to the flexoelectric polarization P_z. Hence, for the same material, the measured d_{33}^{eff} should be proportional to the reciprocal of the product of thickness and curvature radius.

The curvature radius of bent membrane can be obtained from the topographic line profile along diameter of hole and the schematic for curvature radii calculation is shown as the inset in Figure 4b. Radius of curvature R can be calculated by the Pythagorean theorem as $R = \frac{h^2 + (d_0/2)^2}{2h}$, where d_0 is diameter of hole and h is bending depth. Taking curved monolayer MoS_2 membrane as example, d_0 and h obtained from the height profile in Figure 2a are 2.44 µm and 72.2 nm, respectively. Thus, the ideal radius of curvature R is calculated to be 10.3 µm. The roughly calculated curvature radii of bent few-layer MoS_2 and thin-layered InSe flakes are given in Table 1. As illustrated in Figures 2f and 4b, the gray solid lines, which represent thickness dependence of flexoelectric polarization P_z, is consistent with the thickness dependence of measured d_{33}^{eff} value. The results verified that the out-of-plane piezoresponse induced by flexoelectric effect on a curved 2D membrane is proportional to the reciprocal of the product of thickness and curvature radius. Therefore, tuning the curvature of membrane and controlling its thickness have been proven as two available ways to modulate the effective out-of-plane piezoelectricity in 2D materials.

Table 2. A summary of piezoelectric coefficients on 2D van der Waals layered materials in this work and previous works.

Material[a)]	Sample state[a)]	Piezoelectric coefficient	Numerical value [pm V^{-1}]	Refs.
1L MoS_2	Cal.	d_{11}	3.73	[14]
1L MoS_2	Supported by SiO_2	d_{11}	3.78	[40]
1L MoS_2	Supported by Al_2O_3	d_{33}	1.35 ± 0.24	[50]
1L WSe_2	Supported by SiO_2	d_{22}	5.2	[43]
35 nm thick $MoTe_2$	Corrugated	d_{33}	3.98	[51]
1L MoS_2	Suspended	d_{33}	7.5	This work
1L InSe	Cal.	d_{11}	1.46	[20]
1–5L InSe	Cal.	d_{22}	1.86 ± 0.06	[41]
7.5 nm thick InSe	Suspended	d_{33}	21.9	This work

[a)]The abbreviation 1L means monolayer and cal. means calculation.

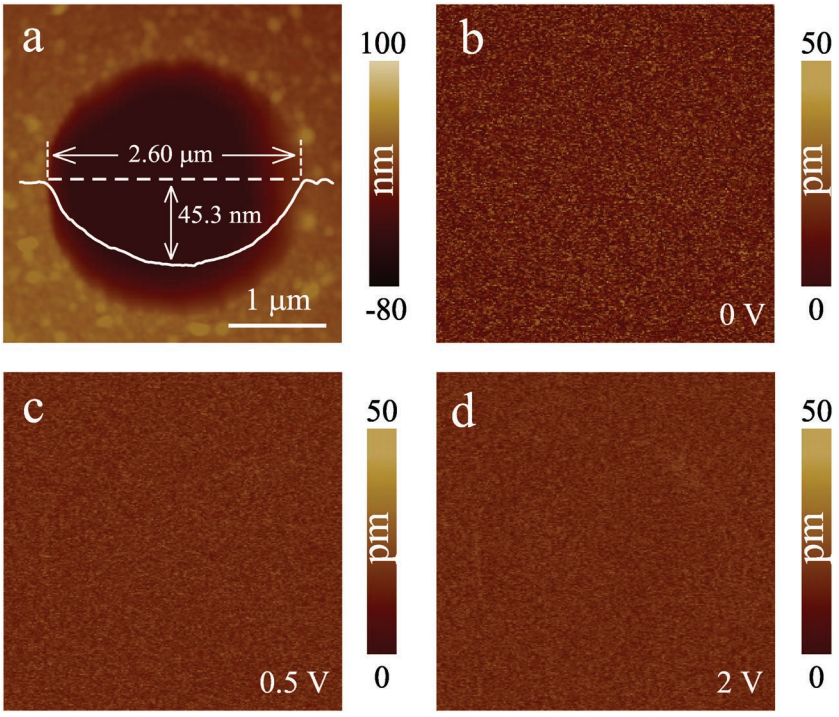

Figure 5. a) The AFM topography of monolayer graphene suspended in the single hole. Out-of-plane piezoresponse amplitude images of monolayer graphene under the driving voltage of b) 0 V, c) 0.5 V, and d) 2 V, respectively.

2.3. Determination of Crosstalk of Surface Topography

Imaging electromechanical property by PFM technique might not only be superimposed by the response of electrostatic effect but also be disturbed by crosstalk of surface topography. Especially, the topographic crosstalk probably makes great influence on the quality of electromechanical images. In present work, the same suspension structure and PFM measurement were implemented on monolayer graphene, so as to examine the interference of topographic crosstalk. It have been theoretically predicted by Zhuang et al. that monolayer graphene possesses a very small flexoelectric coefficient (0.00286 nC m^{-1}) under the prescribed bending deformation, which is less than a tenth of the corresponding coefficient (0.032 nC m^{-1}) of monolayer MoS_2.[60] Hence, monolayer graphene is the appropriate candidate for the controlled trail.

Topographic mapping in **Figure 5**a shows that the suspended single layer graphene membrane presented the similar geometry with bent monolayer MoS_2 membrane, presenting the bent area with the diameter of near 2.6 μm and a flexural depth of about 45 nm. PFM amplitude images of monolayer graphene under drive voltages of 0, 0.5, and 2 V were displayed in Figure 5b–d, respectively. One cannot observe any evident response from PFM amplitudes neither the supported nor free-standing areas of graphene under zero and nonzero bias. Simultaneously, the d_{33}^{eff} coefficient with the value of 0.4 pm V^{-1} measured on bent monolayer graphene was also achieved by linear-fitting the function of averaged piezoresponse amplitudes versus applied AC voltage. The small coefficient may not be faithful due to noise signal and electrostatic effect. However, the result still could indicate that the strain gradient has not induced significant flexoelectricity from the graphene and the crosstalk of surface undulation is inappreciable in the experiments.

3. Conclusion

In the work, we presented a facile method to directly obtain the appreciable effective out-of-plane piezoelectricity and the significant d_{33}^{eff} coefficients of the free-standing monolayer and few-layer MoS_2, as well as thin-layered InSe flakes on the basis of PFM technique. The experiment findings confirmed the d_{33}^{eff} coefficients dominantly arose from electric polarization induced by strain gradient rather than intrinsic in-plane piezoelectricity or other nonpiezoelectric effects, such as electrostatic effect and crosstalk of surface topography. More importantly, based on the experimental conception, the promising effective piezoelectric coefficient of about 21.9 pm V^{-1} on few-layered InSe has first been observed, while the effective out-of-plane piezoelectric coefficient in the monolayer MoS_2 is characterized of about 7.5 pm V^{-1}. Owing to good piezoelectric performance, few-layered InSe films would be considered as one of the next generation ideal candidates for flexible piezotronic/piezophototronic devices with both high sensitivity and good durability. Significantly, the effective out-of-plane piezoresponse induced by flexoelectric effect has been observed on bent MoS_2 with both odd and even number of layers in the present work. It could motivate the potential electric or energy devices to be developed greatly and turn out the chance of commercial batch processes of 2D TMDs piezoelectric materials. Furthermore, the strength of flexoelectricity on curved 2D materials has been verified to be proportional to the reciprocal of the product of thickness and curvature radius. In other words, the strength of flexoelectricity could be modulated by tuning the curvature and thickness of membrane. The present work not only promotes the understanding of electromechanical coupling properties on atomically thin 2D materials, but also could further motivate the development of the potential piezotronic devices.

4. Experimental Section

Fabrication: Low-dimensional 2H-MoS_2 and γ-InSe flakes were prepared and transferred on the perforated sandwich-layered substrates with matrix of circle holes. The holes with diameter of 1–3 μm and depth of 200–300 nm were obtained in the PMMA layer of substrate *via* electron beam lithography (EBL) technique (Pioneer Two, Raith). Compared with conventional perforated silicon based substrate fabrication methods, no reactive ion etching was required in this process. Monolayer 2H-MoS_2 was grown on silicon substrate by chemical vapor deposition (CVD) from MoO_3 solid precursors,[70] while the monolayer graphene was commercially available and also grown by CVD on Cu foils.[71] Then the as-grown monolayer MoS_2 and graphene were transferred on the top

of preprocessed substrates by conventional wet transfer technology.[72] Few-layer 2H-MoS_2 flakes were directly mechanically exfoliated on the preprocessed substrates from a single crystal of bulk 2H-MoS_2 with the assist of scotch tape and polydimethylsiloxane (PDMS).[73] Thin-layered γ-InSe flakes were also prepared by mechanical exfoliation from a single crystal of bulk γ-InSe.

Characterization: Confocal micro-Raman spectrometer (Jobin-Yvon LabRAM HR Evolution, Horiba) with the excitation laser of 532 nm and a commercial AFM system (Dimension Icon, Bruker) using "ScanAsyst-air" AFM tip was used to carefully characterize the morphology and thickness of MoS_2 and InSe flakes. PFM mode was employed to detect the piezoelectricity by a conductive "SCM-PIT" tip coated by Pt/Ir. In order to avoid contact resonance of tip–sample junction, the frequency of applied AC voltage was chosen to be 15 kHz, which was far away from the contact resonance frequency (above 120 kHz).

Supporting Information

Supporting Information is available from the Wiley Online Library or from the author.

Acknowledgements

X.W. and A.Y. C. contributed equally to this work. This work was financially supported by the National Natural Science Foundation of China (grant nos. 91833303 and 61674057), the National Key R&D Program of China (grant nos. 2017YFA0303403 and 2018YFB0406500), Projects of Science and Technology Commission of Shanghai Municipality (grant nos. 18JC1412400, 18YF1407200, and 18YF1407000), and the Program for Professor of Special Appointment (Eastern Scholar) at Shanghai Institutions of Higher Learning. X.W. would like to thank Dr. Ye Yan for a positive discussion on writing the manuscript.

Conflict of Interest

The authors declare no conflict of interest.

Keywords

flexoelectric effect, InSe, MoS_2, piezoelectricity, piezoresponse force microscopy

Received: June 14, 2019
Revised: August 26, 2019
Published online: September 24, 2019

[1] E. W. Hill, A. Vijayaragahvan, K. Novoselov, *IEEE Sens. J.* **2018**, *11*, 3161.
[2] Q. M. Wang, X. H. Du, B. M. Xu, L. E. Cross, *IEEE Trans. Ultrason. Ferroelectr. Freq. Control* **1999**, *46*, 638.
[3] B. Radisavljevic, A. Radenovic, J. Brivio, V. Giacometti, A. Kis, *Nat. Nanotechnol.* **2018**, *6*, 147.
[4] H. Xu, H. M. Zhang, Z. X. Guo, Y. W. Shan, S. W. Wu, J. l. Wang, W. D. Hu, H. Q. Liu, Z. Z. Sun, C. Luo, X. Wu, Z. H. Xu, D. W. Zhang, W. Z. Bao, P. Zhou, *Small* **2018**, *14*, 1803465.
[5] S. Manzeli, D. Ovchinnikov, D. Pasquier, O. V. Yazyev, A. Kis, *Nat. Rev. Mater.* **2017**, *2*, 17033.
[6] M. J. Li, F. S. Yang, Y. C. Hsiao, C. Y. Lin, H. M. Wu, S. H. Yang, H. R. Li, C. H. Lien, C. H. Ho, H. J. Liu, W. W. Li, Y. F. Lin, Y. C. Lai, *Adv. Funct. Mater.* **2019**, *29*, 1809119.
[7] M. J. Li, C. Y. Lin, S. H. Yang, Y. M. Chang, J. K. Chang, F. S. Yang, C. R. Zhong, W. B. Jian, C. H. Lien, C. H. Ho, H. J. Liu, R. Huang, W. W. Li, Y. F. Lin, J. H. Chu, *Adv. Mater.* **2018**, *30*, 1803690.
[8] H. Xu, J. X. Wu, Q. L. Feng, N. N. Mao, C. M. Wang, J. Zhang, *Small* **2014**, *11*, 2300.
[9] D. Jariwala, V. K. Sangwan, L. J. Lauhon, T. J. Marks, M. C. Hersam, *ACS Nano* **2014**, *8*, 1102.
[10] S. Bertolazzi, J. Brivio, A. Kis, *ACS Nano* **2011**, *5*, 9703.
[11] Q. Y. He, Z. Y. Zeng, Z. Y. Yin, H. Li, S. X. Wu, X. Huang, H. Zhang, *Small* **2014**, *8*, 2994.
[12] A. Castellanos-Gomez, M. Poot, G. A. Steele, H. S. J. van der Zant, N. Agrait, G. Rubio-Bollinger, *Adv. Mater.* **2012**, *24*, 772.
[13] W. Z. Wu, L. Wang, Y. L. Li, F. Zhang, L. Lin, S. M. Niu, D. Chenet, X. Zhang, Y. F. Hao, T. F. Heinz, J. Hone, Z. L. Wang, *Nature* **2014**, *514*, 470.
[14] K. A. N. Duerloo, M. T. Ong, E. J. Reed, *J. Phys. Chem. Lett.* **2012**, *3*, 2871.
[15] K. H. Michel, B. Verberck, *Phys. Rev. B* **2011**, *83*, 115328.
[16] M. N. Blonsky, H. L. Zhuang, A. K. Singh, R. G. Hennig, *ACS Nano* **2015**, *9*, 9885.
[17] M. M. Alyörük, Y. Aierken, D. Çaklr, F. M. Peeters, C. Sevik, *J. Phys. Chem. C* **2015**, *119*, 23231.
[18] Y. H. Wang, Z. T. Wang, J. Li, J. Tan, B. Wang, Y. L. Liu, *Phys. Rev. B* **2018**, *98*, 125402.
[19] Y. Guo, S. Zhou, Y. Z. Bai, J. J. Zhao, *Appl. Phys. Lett.* **2017**, *110*, 163102.
[20] W. B. Li, J. Li, *Nano Res.* **2015**, *8*, 3796.
[21] R. Maranganti, P. Sharma, *Phys. Rev. B* **2009**, *80*, 054109.
[22] S. V. Kalinin, A. N. Morozovska, *Nat. Nanotechnol.* **2015**, *10*, 916.
[23] Y. Qi, J. Kim, T. D. Nguyen, B. Lisko, P. K. Purohit, M. C. McAlpine, *Nano Lett.* **2011**, *11*, 1331.
[24] L. E. Cross, *J. Mater. Sci.* **2006**, *41*, 53.
[25] P. Zubko, G. Catalan, A. K. Tagantsev, *Annu. Rev. Mater. Res.* **2013**, *43*, 387.
[26] T. D. Nguyen, S. Mao, Y. W. Yeh, P. K. Purohit, M. C. McAlpine, *Adv. Mater.* **2013**, *25*, 946.
[27] S. V. Kalinin, V. Meunier, *Phys. Rev. B* **2008**, *77*, 033403.
[28] F. Ahmadpoora, P. Sharma, *Nanoscale* **2015**, *7*, 16555.
[29] C. Lee, X. D. Wei, J. W. Kysar, J. Hone, *Science* **2008**, *321*, 385.
[30] Y. H. Li, C. B. Yu, Y. Y. Gan, Y. Y. Kong, P. Jiang, D. F. Zou, P. H. Li, X. F. Yu, R. Wu, H. J. Zhao, C. F. Gao, J. Y. Li, *Nanotechnology* **2019**, *30*, 335703.
[31] A. Lipatov, H. D. Lu, M. Alhabeb, B. Anasori, A. Gruverman, Y. Gogotsi, A. Sinitskii, *Sci. Adv.* **2018**, *4*, eaat0491.
[32] R. Zhang, V. Koutsos, R. Cheung, *Appl. Phys. Lett.* **2016**, *108*, 042104.
[33] B. G. Shin, G. H. Han, S. J. Yun, H. M. Oh, J. J. Bae, Y. J. Song, C. Y. Park, Y. H. Lee, *Adv. Mater.* **2016**, *28*, 9378.
[34] J. Chaste, A. Missaoui, S. Huang, H. Henck, Z. B. Aziza, L. Ferlazzo, C. Naylor, A. Balan, A. T. C. Johnson, R. Braive, A. Ouerghi, *ACS Nano* **2018**, *12*, 3235.
[35] Y. Li, T. M. Wang, M. Wu, T. Gao, Y. W. Chen, R. Sankar, R. K. Ulaganathan, F. C. Chou, C. Wetzel, C. Y. Xu, S. G. Louie, S. F. Shi, *2D Mater.* **2018**, *5*, 021002.
[36] J. J. Qi, Y. W. Lan, A. Z. Stieg, J. H. Chen, Y. L. Zhong, L. J. Li, C. D. Chen, Y. Zhang, K. L. Wang, *Nat. Commun.* **2015**, *6*, 7430.
[37] J. H. Lee, J. Y. Park, E. B. Cho, T. Y. Kim, S. A. Han, T. H. Kim, Y. N. Liu, S. K. Kim, C. J. Roh, H. J. Yoon, H. Ryu, W. Seung, J. S. Lee, J. C. Lee, S. W. Kim, *Adv. Mater.* **2017**, *29*, 1606667.
[38] S. A. Han, T. H. Kim, S. K. Kim, K. H. Lee, H. J. Park, J. H. Lee, S. W. Kim, *Adv. Mater.* **2018**, *30*, 1800342.
[39] S. Manzeli, A. Allain, A. Ghadimi, A. Kis, *Nano Lett.* **2015**, *15*, 5330.
[40] S. K. Kim, R. Bhatia, T. H. Kim, D. Seol, J. H. Kim, H. Kim, W. Seung, Y. Kim, Y. H. Lee, S. W. Kim, *Nano Energy* **2016**, *22*, 483.

[41] M. J. D, Z. G. Wang, F. K. Wang, Y. F. Qiu, J. Zhang, C. Y. Xu, T. Y. Zhai, W. W. Cao, Y. Q. Fu, D. C. Jia, Y. Zhou, P. A. Hu, *Nano Lett.* **2019**, *19*, 5410.
[42] H. Y. Zhu, Y. Wang, J. Xiao, M. Liu, S. M. Xiong, Z. J. Wong, Z. L. Ye, Y. Ye, X. B. Yin, X. Zhang, *Nat. Nanotechnol.* **2015**, *10*, 151.
[43] E. N. Esfahani, T. Li, B. Huang, X. D. Xu, J. Y. Li, *Nano Energy* **2018**, *52*, 117.
[44] X. X. Song, F. Hui, T. Knobloch, B. R. Wang, Z. C. Fan, T. Grasser, X. Jing, Y. Y. Shi, M. Lanza, *Appl. Phys. Lett.* **2017**, *111*, 083107.
[45] X. X. Song, F. Hui, K. Gilmore, B. R. Wang, G. Y. Jing, Z. C. Fan, E. Grustan-Gutierrez, Y. Y. Shi, L. Lombardi, S. A. Hodge, A. C. Ferrarie, M. Lanza, *Nanoscale* **2017**, *9*, 6237.
[46] O. Kolosov, A. Gruverman, J. Hatano, K. Takahashi, H. Tokumoto, *Phys. Rev. B* **1995**, *74*, 4309.
[47] A. Gruverman, M. Alexe, D. Meier, *Nat. Commun.* **2019**, *10*, 1661.
[48] A. Y. Cui, P. De Wolf, Y. Ye, Z. G. Hu, A. Dujardin, Z. Q. Huang, K. Jiang, L. Y. Shang, M. Ye, H. Sun, J. H. Chu, *Nanotechnology* **2019**, *30*, 235701.
[49] Y. Zhou, D. Wu, Y. H. Zhu, Y. J. Cho, Q. He, X. Yang, K. Herrera, Z. D. Chu, Y. Han, M. C. Downer, H. L. Peng, K. J. Lai, *Nano Lett.* **2017**, *17*, 5508.
[50] C. J. Brennan, R. Ghosh, K. Koul, S. K. Banerjee, N. S. Lu, E. T. Yu, *Nano Lett.* **2017**, *17*, 5464.
[51] S. Kang, S. Jeon, S. Kim, D. Seol, H. Yang, J. Lee, Y. Kim, *ACS Appl. Mater. Interfaces* **2018**, *10*, 27424.
[52] K. Lefki, G. J. M. Dormans, *J. Appl. Phys.* **1994**, *76*, 1764.
[53] V. Nagarajan, *Appl. Phys. Lett.* **2005**, *87*, 242905.
[54] H. Li, Q. Zhang, C. C. R. Yap, B. K. Tay, T. H. T. Edwin, A. Olivier, D. Baillargeat, *Adv. Funct. Mater.* **2012**, *22*, 1385.
[55] S. D. Lei, L. H. Ge, S. Najmaei, A. George, R. Kappera, J. Lou, M. Chhowalla, H. Yamaguchi, G. Gupta, R. Vajtai, A. D. Mohite, P. M. Ajayan, *ACS Nano* **2014**, *8*, 1263.
[56] M. H. Zhao, Z. L. Wang, S. X. Mao, *Nano Lett.* **2004**, *4*, 587.
[57] J. A. Christman, R. R. Woolcott, A. I. Kingon, R. J. Nemanich, *Mater. Res. Soc. Symp. Proc.* **1998**, *541*, 617.
[58] N. Syed, A. Zavabeti, J. Z. Ou, M. Mohiuddin, N. Pillai, B. J. Carey, B. Y. Zhang, R. S. Datta, A. Jannat, F. Haque, K. A. Messalea, C. L. Xu, S. P. Russo, C. F. McConville, T. Daeneke, K. Kalantar-Zadeh, *Nat. Commun.* **2018**, *9*, 3618.
[59] C. M. Lueng, H. L. W. Chan, C. Surya, C. L. Choy, *J. Appl. Phys.* **2000**, *88*, 5360.
[60] X. Y. Zhuang, B. He, B. Javvaji, H. S. Park, *Phys. Rev. B* **2019**, *99*, 054105.
[61] M. S. Majdoub, P. Sharma, T. Cagin, *Phys. Rev. B* **2008**, *77*, 125424.
[62] G. W. Mudd, S. A. Svatek, T. Ren, A. Patane, O. Makarovsky, L. Eaves, P. H. Beton, Z. D. Kovalyuk, G. V. Lashkarev, Z. R. Kudrynskyi, A. I. Dmitriev, *Adv. Mater.* **2013**, *25*, 5714.
[63] C. J. Cui, W. J. Hu, X. G. Yan, C. Addiego, W. P. Gao, Y. Wang, Z. Wang, L. Z. Li, Y. C. Cheng, P. Li, X. X. Zhang, H. N. Alshareef, T. Wu, W. G. Zhu, X. Q. Pan, L. J. Li, *Nano Lett.* **2018**, *18*, 1253.
[64] J. A. Christman, R. R. Woolcott, A. I. Kingon, R. J. Nemanich, *Appl. Phys. Lett.* **1998**, *100*, 023114.
[65] X. N. Jiang, W. B. Huang, S. J. Zhang, *Nano Energy* **2013**, *2*, 1079.
[66] D. Errandonea, A. Segura, V. Muñoz, *Phys. Rev. B* **1999**, *60*, 15866.
[67] T. Cheiwchanchamnangij, W. R. L. Lambrecht, *Phys. Rev. B* **2012**, *85*, 205302.
[68] C. Huang, Q. M. Zhang, *Adv. Funct. Mater.* **2004**, *14*, 501.
[69] D. H. Mosca, N. Mattoso, C. M. Lepienski, W. Veiga, I. Mazzaro, V. H. Etgens, M. Eddrief, *J. Appl. Phys.* **2002**, *91*, 140.
[70] Y. N. Liu, R. Ghosh, D. Wu, A. Ismach, R. Ruoff, K. J. Lai, *Nano Lett.* **2014**, *14*, 4682.
[71] K. S. Kim, Y. Zhao, H. Jang, S. Y. Lee, J. M. Kim, K. S. Kim, J. H. Ahn, P. Kim, J. Y. Choi, B. H. Hong, *Nature* **2009**, *457*, 706.
[72] J. W. Suk, A. Kitt, C. W. Magnuson, Y. F. Hao, S. Ahmed, J. H. An, A. K. Swan, B. B. Goldberg, R. S. Ruoff, *ACS Nano* **2011**, *5*, 6916.
[73] Y. Huang, E. Sutter, N. N. Shi, J. B. Zheng, T. Z. Yang, D. Englund, H. J. Gao, P. Sutter, *ACS Nano* **2015**, *9*, 10612.